Chemical Science

ROYAL SOCIETY OF CHEMISTRY

EDGE ARTICLE

View Article Online
View Journal | View Issue

Cite this: *Chem. Sci.*, 2025, **16**, 2673

All publication charges for this article have been paid for by the Royal Society of Chemistry

Received 13th August 2024
Accepted 12th December 2024

DOI: 10.1039/d4sc05428h

rsc.li/chemical-science

Enhancement of photoinduced reactive oxygen species generation in open-cage fullerenes†

Cristina Castanyer,‡[a] Çetin Çelik, ‡[b] Albert Artigas, [a] Anna Roglans, [a] Anna Pla-Quintana, *[a] Anton J. Stasyuk, *[acd] Yoko Yamakoshi *[b] and Miquel Solà *[a]

Photodynamic therapy is an important tool in modern medicine due to its effectiveness, safety, and the ability to provide targeted treatment for a range of diseases. Photodynamic therapy utilizes photosensitizers to generate reactive oxygen species (ROS). Fullerenes can be used as photosensitizers to produce ROS in high quantum yields. Open-cage fullerenes are a subclass of fullerenes characterized by a partially open structure, with one or more openings or apertures. The promising electrochemical properties of open-cage fullerenes motivated us to investigate their use for DNA-cleavage and ROS generation under visible light irradiation through type I electron transfer and type II energy transfer reactions. Our results show that open-cage C_{60} fullerenes are more efficient for photoinduced cleavage of DNA and ROS generation *via* both the type I electron transfer and type II energy transfer pathways than pristine C_{60} or a C_{60} pyrrolidine derivative without open-cage. The greater efficiency of ROS generation by open-cage C_{60} fullerene in type I and type II reactions can be attributed to the increased rate of the initial intersystem crossing process, resulting from larger total reorganization energies, as indicated by computationally calculated relative rates using the Marcus equation, and the lower reduction potential of the open-cage derivative **3**, as determined by CV, which facilitates a more efficient generation of the corresponding radical anion ($C_{60}^{\bullet-}$).

Introduction

Photodynamic therapy (PDT),[1–3] discovered over a century ago, has evolved into a well-established treatment for cancer and infections.[4–6] PDT involves the use of photosensitizers (PSs),[7,8] which are non-toxic dyes activated by light absorption. This activation first forms an excited singlet state of the PS, which then transitions to a long-lived excited triplet state (Scheme 1). In the presence of oxygen, the triplet state undergoes photochemical reactions, producing reactive oxygen species (ROS) that can destroy cancer cells, pathogenic microbes, and unwanted tissue.

Fullerene C_{60} is particularly well-suited PS for PDT due to its ability to generate ROS in high quantum yields.[9–11] However, its hydrophobic nature and poor solubility in biological media have hindered the biomedical applications of fullerenes in its pristine form. Therefore, significant efforts have been made over the years to synthesize PSs based on water-soluble fullerene derivatives.[12] As one of the highly suited derivatives, polyhydroxy fullerenes (fullerols)[13,14] were reported with enhanced aqueous solubility, however, their precise structure often remains unknown. To synthesize water-soluble C_{60} derivatives with well-defined structures, two synthetic methods were mainly employed; Bingel–Hirsch cycloaddition reaction[15,16] and 1,3-dipolar cycloaddition (Prato reaction).[17] Using the former reaction, fullerene carboxylic acid derivatives[18,19] and the latter, fullerene quaternary ammonium derivatives[20,21] were reported as water-soluble derivatives resulting in recent studies with further advanced properties[22–27] in combination with biomolecules, including sugars[24,25] and peptides,[28] polymers,[29,30] and nanoparticles.[31,32] Despite these intensive reports on C_{60}-based PDT-PS, to date, there have been no studies on open-cage fullerene derivatives reported in this context.

Fullerene-based PSs offer considerable advantages over conventional PSs based on the suitable properties of C_{60} with (1)

[a]*Institut de Quimica Computacional i Catàlisi (IQCC) and Departament de Química, Universitat de Girona, M. Aurèlia Capmany, 69, 17003 Girona, Catalonia, Spain. E-mail: anna.plaq@udg.edu; antony.stasuk@gmail.com; miquel.sola@udg.edu*

[b]*Department of Chemistry and Applied Biosciences, ETH Zürich, Vladimir-Prelog-Weg 3, CH-8093 Zürich, Switzerland. E-mail: yamakoshi@org.chem.ethz.ch*

[c]*Faculty of Chemistry, University of Warsaw, Pasteura 1, 02-093 Warsaw, Poland*

[d]*Departament de Farmàcia i Tecnologia Farmacèutica, i Fisicoquímica, Facultat de Farmàcia i Ciències de l'Alimentació & Institut de Química Teòrica i Computacional (IQTCUB), Universitat de Barcelona (UB), Av. Joan XXIII 27-31, Barcelona, Catalonia, Spain*

† Electronic supplementary information (ESI) available: Details of the synthesis of **1–3** and preparation of **P1–3** complexes with corresponding spectral data, experimental methods for DNA cleavage tests, and ESR spin-trapping methods. Computational details, energies of lowest-lying S_1 and T_1 excited states estimated in Franck–Condon and relaxed geometries, and Gibbs energy ΔG^0, and total reorganization energy λ_t, for ISC type II, and type I reactions. See DOI: https://doi.org/10.1039/d4sc05428h

‡ These authors contributed equally to this work.

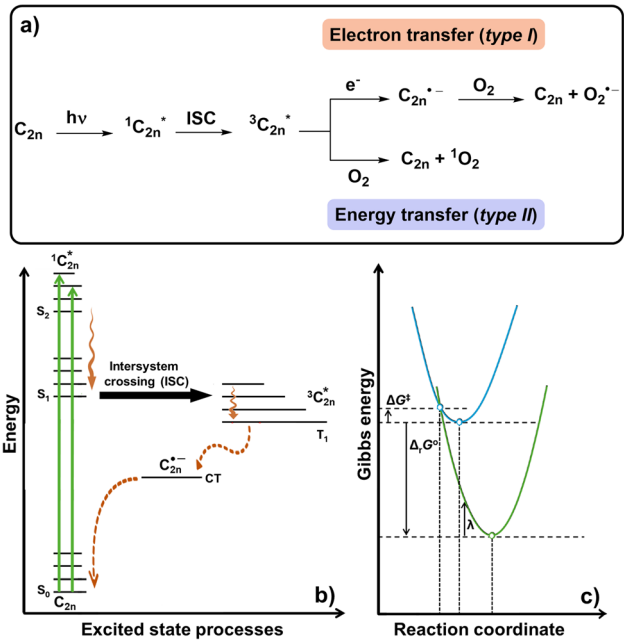

Scheme 1 (a) Photoinduced reactive oxygen species generation from fullerenes (C_{60} and C_{70}) *via* electron transfer (type I) and energy transfer (type II) pathways. (b) Schematic representation of the excited state processes that take place from C_{2n} to $^3C^*_{2n}$ (types I and II) and from here to $C_{2n}^{\bullet-}$ (type I). (c) Marcus parabolic model describing the charge transfer from a D–A (donor–acceptor, blue curve) to D^+–A^- (green curve).

high photostability and reduced photobleaching and (2) quantitative singlet oxygen ($^1O_2$) generation having a quantum yield of close to 1.[9] Notably, C_{60} follows two photophysical mechanisms for ROS generation – type I electron transfer and type II energy transfer (Scheme 1a), whereas conventional PDT dyes mainly rely on a single mechanism with type II. In type I electron transfer,[10,33] the fullerene in its triplet excited state ($^3C^*_{60}$), which has a relatively high redox potential ($^3C^*_{60}$: $E_1 = +1.14$ V *vs.* SCE in PhCN), interacts with an electron donor such as NADH to form the radical anion $C_{60}^{\bullet-}$, which further produces $O_2^{\bullet-}$ (Scheme 1b), the ROS which can be subsequently converted to the most toxic ROS, $^{\bullet}OH$, by the Fenton reaction. Alternatively, in the type II energy transfer pathway, $^3C^*_{60}$ reacts with O_2 to generate $^1O_2$, another ROS.[9,34] Rates of these two processes can be estimated using the Marcus parabolic model (Scheme 1c).[35,36]

Previously, we have observed the generation of $O_2^{\bullet-}$ and $^{\bullet}OH$ in aqueous solution of C_{60} complexed with poly(vinylpyrrolidone) (PVP) by means of electron spin resonance (ESR) spin-trapping methods under visible light irradiation.[37,38] More recently, we have reported on the photoinduced oxidative DNA damage and related ROS generations by water-soluble C_{60}-PEG and two isomeric C_{70}-PEG derivatives[39] with fulleropyrrolidine skeletons.[40] It was found that the photoinduced cleavage of DNA by C_{60}-PEG *via* type I electron transfer is much higher than that by C_{70}-PEG, whereas the reverse is true for type II energy transfer.[30] Computationally estimated relative rates of each step of the type I and type II reactions were able to explain the differences in photoinduced ROS generation of C_{60}-PEG and C_{70}-PEG in water.

Open-cage fullerenes are known as interesting molecules due to their unique shapes and properties. They are obtained by selective cleavage of one or more C–C bonds of the fullerene cage. Once opened, these fullerenes can act as host molecules encapsulating guests within their cavity. In the molecular surgery procedure,[41] the fullerene is first opened, then a guest molecule is introduced in the cavity, and finally the structure is closed to generate an endohedral fullerene. Some open-cage derivatives of C_{60} were found useful as electron accepting materials in organic solar cells.[42]

In 2018, we prepared bis-fulleroid derivatives by a Rh-catalyzed [2+2+2] cycloaddition of diynes and C_{60} to yield a cyclohexadiene-fused intermediate, which transformed into a bis-fulleroid through a [4+4]/retro-[2+2+2] rearrangement.[43,44] The obtained bis-fulleroid can overcome ring expansion through a photooxygenation process to deliver an open-cage derivative with a 12-membered hole in the C_{60} cage structure. The same procedure was applied to open an orifice in C_{70}.[45] The obtained open-cage C_{60} derivatives above were incorporated in perovskite solar cells as an electron transport layer (ETL), resulting in solar cells with higher performances than those of previously reported solar cells containing standard $PC_{61}BM$ material as ETL.[42] The improved performance of this open cage C_{60} derivative was attributed, at least in part, to the increased energy levels of the HOMO and LUMO orbitals due to the open cage structure.

The promising electrochemical properties and remarkable stability of these open-cage C_{60} above prompted us to study these compounds for their photoinduced ROS generation *via* type I electron transfer and type II energy transfer. To this end, we considered to test on C_{60} and three C_{60} derivatives **1–3** shown in Fig. 1. To have more bio-relevant conditions, we prepared water-soluble complexes of C_{60} and compounds **1–3** with PVP (**C_{60}/PVP**, **P1**, **P2**, and **P3**) and tested by photoinduced oxidative DNA damages. The generation of responsible ROS ($^1O_2$ and $O_2^{\bullet-}$) by **C_{60}/PVP** and complexes **P1–3** were measured by ESR in the presence of spin-trapping agents. Finally, computational calculations were performed to investigate the relative reaction rate of each step to understand the mechanisms in ROS generation from C_{60} and **1–3** derivatives.

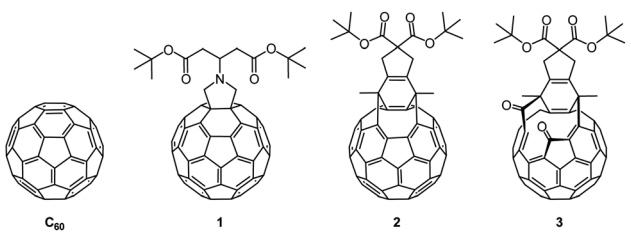

Fig. 1 Molecular structure of the C_{60} and C_{60} derivatives **1–3**. The water-soluble complex of each compound with poly(vinylpyrrolidone) (PVP) (**C_{60}/PVP**, **P1**, **P2**, or **P3**) was prepared for DNA cleavage tests and ROS generation measurements.

Results and discussion

Preparation of water-soluble complexes of C_{60} and C_{60} derivatives 1–3 with PVP

A fulleropyrrolidine derivative **1** (ref. 46) and two open cage C_{60} derivatives **2** and **3** (ref. 42 and 44) were synthesized based on the reported procedures. The UV-vis absorption spectra for the three compounds were registered showing the intense absorption in the UV region and lower intensity broad bands in the visible region, with the expected characteristic bands (430 nm for **1**; 259 and 325 nm for **2**; and 254 and 324 nm for **3**, see Fig. S1–S3†). Cyclic voltammetry was also recorded for the three compounds showing first reduction potentials of −1.18 V for **1**, −1.26 V for **2** and −1.06 V for **3** (see Fig. S4–S9†). These data altogether also allowed us to experimentally determine the HOMO and LUMO energies for the three compounds (see Table S1†).

Since these compounds were not soluble in water, aqueous solutions of C_{60} and compounds **1–3** were prepared by forming complexes with a neutral polymeric detergent, PVP, as described in the literature.[47] Each PVP complex, **C_{60}/PVP**, **P1**, **P2**, or **P3**, was water-soluble and revealed sufficient absorption intensity in visible wavelength region (Fig. S10†), showing good potentials as PDT-PSs. The characteristic bands of the absorption spectra were not altered by the presence of the PVP especially in the visible region, suggesting that the photophysical processes remain unaffected by the presence of PVP (see Fig. S11–S13†).

Photoinduced ROS ($^1O_2$ and $O_2^{\bullet-}$) generation

Generation of ROS from the photoexcited **C_{60}/PVP** and **P1–3** complexes were investigated by ESR spin trapping methods. $^1O_2$ generation *via* type II energy transfer reaction (see Scheme 1) by each compound was measured using a spin-trapping reagent, 4-oxo-TEMP (scheme in Fig. 2a bottom). Peaks corresponding to the $^1O_2$ adduct of 4-oxo-TEMP (4-oxo-TEMPO) were observed in all solutions after irradiation by green LED light (528 nm max) for 10 min (Fig. 2a). Fig. 2b (upper) shows double integration analyses of the ESR signal to estimate the relative amount of $^1O_2$ generation. The results revealed that the generation of $^1O_2$ by bis-fulleroid **P2** and open-cage **P3** were significantly higher than that of unsubstituted C_{60}, which was in parallel with the absorption intensity at 528 nm varies in the order **P1** ≈ **P2** > **P3** > **C_{60}/PVP** (Fig. S10†). Despite **P1** having relatively higher absorbance at this wavelength, it revealed only slightly higher $^1O_2$ generation than C_{60}. Generation of $^1O_2$ was observed in an irradiation-time-dependent manner in all complexes (Fig. 2b bottom, Fig. S14–S17†), clearly indicating that $^1O_2$ generations were due to the photoexcitation of **C_{60}/PVP**, **P1**, **P2**, and **P3**. The fact that **P2** and **P3** show almost identical behaviour can be explained by the facile transformation of **2** into **3** in the presence of light and oxygen.

The generation of the other ROS, $O_2^{\bullet-}$, which can be produced *via* type I electron transfer pathway (Scheme 1) by photoexcited **C_{60}/PVP** and complexes **P1–3**, was investigated in the presence of electron donor NADH using DEPMPO as a spin trapping reagent (scheme in Fig. 3a bottom). Upon irradiation with green LED, all complexes showed $O_2^{\bullet-}$ generation in aqueous media observed as signals of DEPMPO-OOH (Fig. 3a). When the ESR spectra were quantified by double integration, the relative amount of $O_2^{\bullet-}$ produced by each complex was clearly estimated (Fig. 3b). The amount of $O_2^{\bullet-}$ generation was in a similar trend to that of $^1O_2$ generation; **P2** and **P3** had much higher generation than **C_{60}/PVP** system and **P1** (Fig. 3b). The irradiation-time-dependency was also observed as shown in Fig. 3c and S18–S21.† It is known that $O_2^{\bullet-}$ can be produced not only *via* the type I pathway but also *via* $^1O_2$, which was once generated through the type II energy transfer pathway, in the presence of electron donors. To detect the $O_2^{\bullet-}$ generated exclusively *via* the type I electron transfer pathway, ESR experiments in the presence of L-histidine (His), a $^1O_2$ quencher, were performed. As shown in Fig. 3b, the reduced amount of $O_2^{\bullet-}$ generation was observed in all complexes in the presence of His, while **P2** showed only a limited amount of decrease (Fig. 3b). This was presumably due to the rapid reaction of **P2** with $^1O_2$ to form **P3**, effectively quenching this species. However, the possibility of a faster rate for the type I pathway reaction relative to the type II pathway cannot be ruled out.

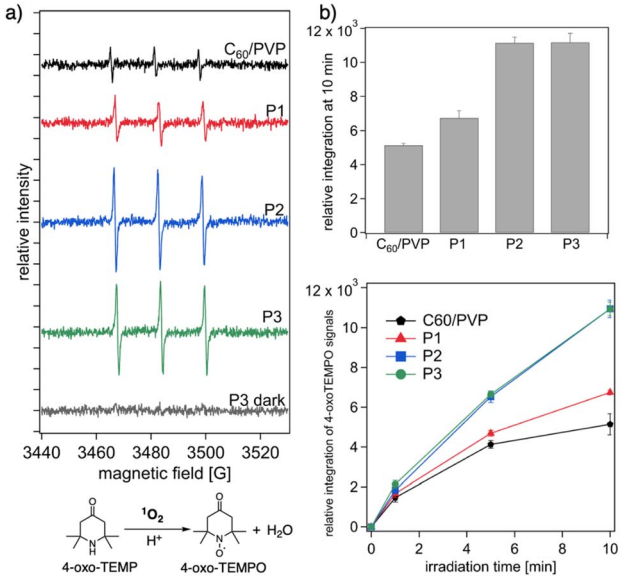

Fig. 2 Photoinduced generations of $^1O_2$ by **C_{60}/PVP** and **P1–P3** in aqueous solutions. (a) X-band ESR spectra of $^1O_2$ adduct of 4-oxo-TEMP generated in aqueous solution of **C_{60}/PVP**, **P1**, **P2**, and **P3**, under photoirradiation for 10 min and scheme for the reaction of $^1O_2$ with a spin trapping reagent, 4-oxo-TEMP. (b) Relative amount of $^1O_2$ generation estimated by double integration of the peaks corresponding to 4-oxo-TEMPO after 10 min irradiation (upper) and from time-dependent measurements (lower). C_{60} or C_{60} derivatives **1–3**: 40 μM; 4-oxo-TEMP: 80 mM; in 60 mM phosphate buffer (pH 7.0). Photoirradiation conditions: green LED (528 nm, 93 lm W^{-1}), 4 cm distance, room temperature, 0–10 min. Measurement conditions: temperature 298 K; microwave frequency 9.78 GHz; microwave power 10 mW; receiver gain 5.02×10^4; modulation amplitude 1.00 G; modulation frequency 100 kHz; sweep time 83.89 s. Measurements were triplicated.

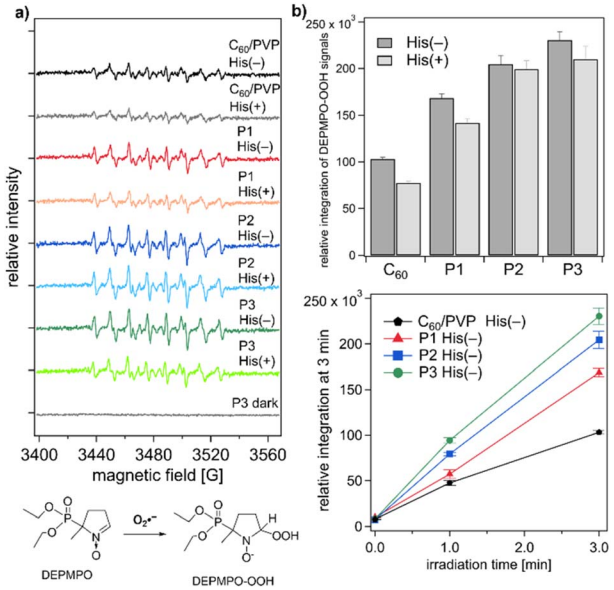

Fig. 3 Photoinduced generations of $O_2^{\bullet-}$ by **C_{60}/PVP** or **P1–3** in aqueous solutions. (a) X-band ESR spectra of $O_2^{\bullet-}$ adduct of DEPMPO in aqueous solution of **C_{60}/PVP**, **P1**, **P2**, and **P3**; and scheme for the reaction of $O_2^{\bullet-}$ with a spin trapping reagent, DEPMPO. (b) Relative amount of $O_2^{\bullet-}$ generation estimated by double integration of the peaks corresponding to DEPMPO-OOH. C_{60} or C_{60} derivatives **1–3**: 40 μM; DETAPAC: 1 mM; NADH: 10 mM; L-histidine: 10 mM; DEPMPO: 113 mM; in phosphate buffer (60 mM, pH 7.0). Photoirradiation conditions: green LED (528 nm, 93 lm W^{-1}), 4 cm distance, room temperature, 0–3 min. Measurement conditions: temperature 298 K; microwave frequency 9.78 GHz; microwave power 10 mW; receiver gain 5.02 × 10^4; modulation amplitude 1.00 G; modulation frequency 100 kHz; sweep time 83.89 s. Measurements were triplicated.

Photoinduced DNA cleavage

In order to evaluate their potential as PDT-PSs, a photo DNA cleavage assay was performed using **C_{60}/PVP** and **P1–3.** Supercoiled pBR322 DNA was used as a DNA substrate to observe the DNA cleavage ability of the compounds by quantifying the amount of damaged DNA (form II nicked DNA) in relative to the intact ones (form I). Under visible light irradiation (green LED 527 nm), cleavages of the DNA by all four complexes were observed (Fig. 4 and S23–S26†). **P2** and **P3** showed stronger DNA cleavage upon photo irradiation than that of **C_{60}/PVP** and **P1.** These results were in line with the ROS generation measured by ESR spin trapping methods, where **P2** and **P3** showed higher generation of both $^1O_2$ and $O_2^{\bullet-}$ than **C_{60}/PVP** and **P1.** We also observed that DNA cleavage in absence of NADH was significantly lower in all compounds, suggesting that type I pathway plays a crucial role in photoinduced DNA damage, assuming that $^1O_2$ and $O_2^{\bullet-}$ have an analogous damage power. Noteworthy, generation of form II nicked DNA in the absence of NADH is significantly higher for **P3** than the other compounds including **C_{60}/PVP**, which indicates increased involvement of ROS generation by type II pathway from this complex in relation to others.

Quantum chemical modelling

To further investigate the mechanism of ROS generation from considered open cage fullerenes through the type I and type II

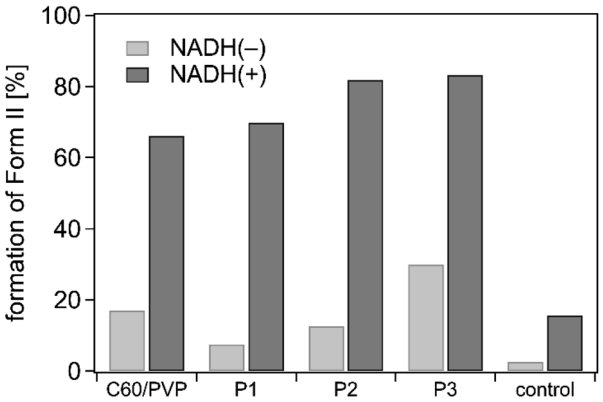

Fig. 4 Photoinduced DNA cleavage by **C_{60}/PVP** and **P1–3** in the absence or presence of NADH as an electron donor. Data is obtained from gels shown in Fig. S11 and S12 in the ESI.† Reaction conditions: pBR322: 25 ng μL^{-1}; **C_{60}/PVP** or **P1–3**: 0.125 mM; NADH: 10 mM; in Tris–HCl buffer (pH 8.0, 1 mM EDTA); green LED (527 nm, 45 lm W^{-1}), at room temperature, for 25 min. Electrophoresis: 100 V, 80 min, 1% agarose in 0.5× TBE buffer (pH 8.3).

reactions, computational calculations were performed. Taking into account the moderate size of the studied systems, C_{60} fullerene as well as derivatives **1–3** were considered without any simplification. The NADH structure was replaced with a model compound represented by one nucleoside containing only nicotinamide as the base (see Fig. S15†). The applicability of such a replacement for the sake of simulation of photoinduced reactive oxygen generation has been previously demonstrated by us.[30] The rate of excited state processes, including intersystem crossing (ISC), type II (energy transfer), and type I (electron transfer), both part 1 and part 2 (schemes in Tables 1 and 2), were estimated using the classical Marcus equation:[48]

$$k_{ET} = \frac{2\pi}{\hbar}|H_{AB}|^2 \frac{1}{\sqrt{4\pi\lambda_t k_b T}} \exp\left(\frac{-(\lambda_t + \Delta G^0)^2}{4\lambda_t k_b T}\right) \quad (1)$$

where $|H_{AB}|$ is the electronic matrix element describing the electronic coupling between the electronic states of the reactants and the products, ΔG^0 is the Gibbs energy, and λ_t is the total reorganization energy. λ_t is the sum of two components,

Table 1 Sum of Gibbs energies and total reorganization energies ($\Delta G^0 + \lambda_t$) in eV and relative rates (F = fast, M = medium, S = slow) for ISC and type II reaction estimated with respect to reference C_{60} fullerene

	ISC		Type II	
Compounds	($\Delta G^0 + \lambda_t$)	Rel. rate	($\Delta G^0 + \lambda_t$)	Rel. rate
1	−0.345	M	−0.097	F
2	−0.109	F	−0.037	F
3	−0.240	F	0.095	F
C_{60}	−0.411	S	−0.282	S

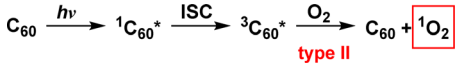

Table 2 Sum of Gibbs energies and total reorganization energies ($\Delta G^0 + \lambda_t$) in eV and relative rates (F = fast, M = medium, S = slow) for ISC and type I reaction (part 1 and part 2) estimated with respect to reference C_{60} fullerene

			Type I			
	ISC		Part 1		Part 2	
	($\Delta G^0 + \lambda_t$)	Rel. rate	($\Delta G^0 + \lambda_t$)	Rel. rate	($\Delta G^0 + \lambda_t$)	Rel. rate
1	−0.345	M	0.418	M	0.295	F
2	−0.109	F	0.584	S	0.230	F
3	−0.240	F	0.412	M	0.485	M
C_{60}	−0.411	S	0.273	F	0.445	M

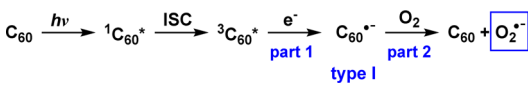

the internal reorganization energy (λ_i) and the external reorganization energy (λ_s). In accordance with Marcus theory, the dependence between the electron/energy transfer (ET/EnT) rate and driving force (ΔG^0) is described by a Gaussian function. The rate increases with the driving force until the reaction's reorganization energy matches the driving force ($\Delta G^0 = -\lambda_t$). Further increase in the driving force leads to a decrease in the ET rate in the so-called Marcus inverted region. A detailed description of reorganization energy estimation is provided in the computational details section in the ESI.† It is well known that $|H_{AB}|$ values are very sensitive to the mutual orientation of the species involved in ET/EnT processes. Their precise estimation is especially problematic for intermolecular processes where the relative position of donor and acceptor sites can vary in a wide range. The structural similarity of the systems under consideration allowed us to also assume the similarity of effective $|H_{AB}|$ values. This assumption, in turn, allowed us to estimate relative rates with respect to reference C_{60} fullerene (eqn (2)).

$$\frac{k_{ET}^{P_x}}{k_{ET}^{C_{60}}} \cong \exp\left(\frac{\left(\lambda_t^{C_{60}} + \Delta G^{0,C_{60}}\right)^2}{\lambda_t^{C_{60}}} - \frac{\left(\lambda_t^{P_x} + \Delta G^{0,P_x}\right)^2}{\lambda_t^{P_x}}\right) \quad (2)$$

Taking into account that the sizes of **1–3** conjugates are relatively small, the effect of geometrical relaxation in the corresponding excited state can be significant and must be properly accounted for. Indeed, comparison of excited state energies for **1–3** fullerenes in vertical ground state geometries and equilibrium first excited state geometries revealed that the difference was 0.48–0.63 eV and 0.45–0.59 eV for singlet and triplet states, respectively (Table S1, ESI†). Thus, for all studied processes, geometry relaxation in the corresponding excited state was accounted for accordingly.

In accordance with Scheme 1, the photoinduced reactive oxygen species generation is a sequential process consisting of photoexcitation and ISC stages followed by ET or EnT processes. As seen in Fig. S1,† the absorbance of **1–3** derivatives is 1.37 to 1.84 times higher than that of the parental C_{60} fullerene. Thus, the initial stage of reactive oxygen generation for the systems of interest is expected to be more efficient compared to C_{60}.

Analyses of ($\Delta G^0 + \lambda_t$) as well as relative rates for ISC and type II energy transfer are summarized in Table 1. The Gibbs energy for triplet-to-singlet oxygen conversion ($^3O_2(^3\Sigma_g) \rightarrow {}^1O_2(^1\Delta_g)$) process was taken from experiment.[49]

For all studied systems, the ISC reaction occurs in the inverted Marcus region ($|\Delta G^0| > \lambda_t$). ISC rates for **2** and **3** are predicted to be the fastest among the systems. At the same time, ($\Delta G + \lambda_t$) values for C_{60} and the **1** conjugate are significantly higher, suggesting their slower ISC rates. Table S2 in ESI† contains the individual ΔG^0 and λ_t values for the ISC and type II reaction, for the systems of interest. The type II energy transfer for **1–3** conjugates is characterized by very small ($\Delta G + \lambda_t$) values, suggesting a nearly barrierless process with a fast reaction rate. In contrast, the type II reaction in the reference C_{60} occurs in inverted region and is expected to be slower as compared to **1–3**. Taking into account that ISC and $^1O_2$ generation are two linked and consecutive reactions, where the product of the first reaction serves as the substrate for the second one, it can be argued that the rate of the entire process is determined by the rate of the slowest reaction. The experimentally observed more efficient $^1O_2$ generation by **P2** and **P3** complexes, followed by **P1** and C_{60} (**P2** > **P3** > **P1** > **C_{60}/PVP**), together with the fact that the absorption intensity at 528 nm varies in the order **P1** ≈ **P2** > **P3** > C_{60} (and thus does not correctly describe the observed order) allows us to assume that the ISC stage is the rate-determining step. Interestingly, **2** and **3** have relatively large total reorganization energies as compared to **1** and C_{60} for the ISC step, which translates into relatively low ($\Delta G^0 + \lambda_t$) values.

The photoinduced ROS generation that proceeds through electron transfer reaction (type I reaction) can be divided into two steps. The first step (part 1) is the reduction of fullerene by the electron transfer from NADH. The second step (part 2) is the reduction of molecular oxygen and generation of the superoxide radical ion $O_2^{\bullet-}$ (see Table 2 footnote). Analyses of ($\Delta G^0 + \lambda_t$) and relative rates for the initial ISC process and the two subsequent steps of the type I reaction are summarized in Table 2. Individual ΔG^0 and λ_t values for the ISC and both stages of the type I reaction are provided in Table S2, ESI.†

In contrast to the type II reaction, both part 1 and part 2 stages of the type I reaction take place in the normal Marcus region ($|\Delta G^0| < \lambda_t$). Similar to the generation of $^1O_2$, the type I reaction and the preceding ISC are linked reactions, and the rate-determining stage will be the slowest one. Following the experimental results of $O_2^{\bullet-}$ generation in the presence of the electron donor NADH, the bis-fulleroid **P2** and open-cage fullerene **P3** demonstrated a superior capability for superoxide generation compared to the closed-cage **P1** and the parental C_{60}. Additionally, the **P1** conjugate outperformed C_{60}. The observed efficiency of the studied systems towards $O_2^{\bullet-}$ radical anion generation suggested that in the case of the type I reaction, again ISC was the slowest, and thus the rate-determining stage. Experimental support for the relative rates determined for type I part 1 can be found in the determined reduction potentials that vary in the order **3** < **1** < **2**.

Conclusions

Four types of water-soluble complexes of C_{60} and C_{60} derivatives (**1–3**) with PVP (**C_{60}/PVP** and **P1–3**) were prepared and tested for oxidative damage of DNA and responsible ROS generation under visible light irradiation. While compound **1** is a standard fulleropyrrolidine derivative, compounds **2** and **3** are bis-fulleroid and open-cage fullerene, respectively. Our results show that species **2** and **3** are more efficient than **1** and C_{60} for both the generation of $O_2^{\bullet-}$ *via* type I electron transfer pathway and the generation of $^1O_2$ and *via* type II energy transfer reaction in line with the results of photo DNA cleavage by these compounds. The highly efficient generation of ROS by **2** and **3** in type I and type II reactions was explained by (1) the higher rate for the initial ISC process due to larger total reorganization energies of **2** and **3**, as shown by computational results based on Marcus equation, and (2) the reduced reduction potential of open-cage derivative **3**, as determined by CV. These altogether allow a more efficient generation of the corresponding anion radical ($C_{60}^{\bullet-}$). Since **2** can be easily converted into **3** upon light and oxygen exposure, **3** is the best candidate for PDT identified in this study, highlighting the potential of open-cage derivatives for the development of more efficient photosensitizers in photodynamic therapy.

Experimental

General

Unless otherwise noted, materials were obtained from commercial suppliers and used without further purification. All ^{1}H and ^{13}C NMR spectra were recorded on a Bruker ASCEND 400 spectrometer equipped with a 5 mm BBFO probe or and Bruker 600 spectrometer equipped with a CryoProbe using $CDCl_3$ as a deuterated solvent. Mass spectrometry analyses were recorded on a Bruker micrOTOF-Q II mass spectrometer (high resolution), equipped with electrospray ion source and a Bruker Daltonics solariX spectrometer.

Synthetic methods

Synthesis of 1, 2, and 3. Compound **1** was prepared by reported methods.[46] Spectroscopic data for **1**: ^{1}H NMR ($CDCl_3$, 400 MHz) δ (ppm): 1.57 (s, 18H), 2.80 (dd, J = 15.0, 6.6 Hz, 2H), 2.98 (dd, J = 15.0, 6.6 Hz, 2H), 4.21 (quint, J = 6.6 Hz, 1H), 4.55 (s, 4H); ^{13}C NMR ($CDCl_3$, 150 MHz) δ (ppm): 28.4, 38.5, 54.8, 63.3, 69.9, 81.4, 136.6, 140.3, 142.0, 142.2, 142.3, 142.8, 143.2, 144.7, 145.4, 145.6, 145.9, 146.1, 146.2, 146.4, 147.5, 154.9, 171.1; ESI-HRMS (m/z) calculated for $[M + H]^+$ = 1006.2013; found 1006.2002. Compounds **2** and **3** were prepared following reported methods for similar derivatives.[42,44] Spectroscopic data for **2**: ^{1}H NMR ($CDCl_3$, 400 MHz) δ (ppm): 1.49 (s, 9H), 1.54 (m, 9H), 2.88 (s, 6H), 3.21–3.27 (m, 2H), 3.34–3.40 (m, 2H); ^{13}C NMR ($CDCl_3$, 101 MHz) δ (ppm): 27.92, 27.95, 28.1, 39.9, 44.4, 59.8, 81.7, 81.8, 126.7, 135.2, 135.7, 136.5, 136.8, 137.1, 137.6, 139.0, 139.1, 140.0, 140.1, 140.5, 140.9, 143.3, 143.4, 143.6, 143.7, 143.8, 143.9, 144.0, 144.4, 144.5, 144.6, 144.7, 145.2, 145.3, 145.7, 145.8, 149.8, 151.8, 170.6, 170.9; ESI-HRMS (m/z) calculated for $[M + Na]^+$ = 1063.1880; found 1063.1877. Spectroscopic data for **3**: ^{1}H NMR ($CDCl_3$, 400 MHz) δ (ppm): 1.60 (s, 9H), 1.68 (s, 9H), 2.29 (s, 3H), 2.63 (s, 3H), 3.44 (d, J = 16.0 Hz, 1H), 3.72 (d, J = 16.8, 1H), 4.05 (d, J = 16.0 Hz, 1H), 4.34 (d, J = 16.8, 1H); ^{13}C NMR ($CDCl_3$, 101 MHz) δ (ppm): 28.2, 28.3, 32.0, 32.3, 40.3, 41.6, 43.6, 52.4, 60.3, 81.5, 129.3, 131.6, 131.8, 132.0, 132.3, 133.2, 133.3, 135.4, 135.8, 135.9, 136.2, 136.3, 136.7, 137.12, 137.13, 137.6, 137.8, 138.8, 139.7, 140.0, 140.3, 140.4, 140.5, 140.6, 140.9, 141.0, 141.3, 141.8, 142.0, 142.5, 142.8, 142.9, 143.0, 144.2, 144.4, 144.5, 144.73, 144.75, 145.24, 145.25, 145.5, 145.78, 145.80, 145.86, 145.91, 145.94, 146.0, 146.08, 146.13, 146.2, 146.4, 146.5, 147.1, 147.5, 147.8, 147.89, 147.93, 148.8, 150.0, 151.1, 155.9, 170.7, 172.3, 191.4, 202.6; ESI-HRMS (m/z) calculated for $[M + Na]^+$ = 1095.1778; found 1095.1768.

Preparation of PVP complexes C_{60}/PVP and P1–3. Water soluble complexes were prepared by complexation of C_{60} and compounds **1–3** with PVP (**C_{60}/PVP**, **P1**, **P2**, and **P3**) following the reported method.[47] C_{60} or C_{60} derivatives **1–3** (0.0011 mmol) were dissolved in toluene (1.0 ml) and 2.0 ml of $CHCl_3$ containing 100 mg of PVP (K-30) was added. The resulting solution was sonicated for one hour and the solvents were then slowly evaporated under vacuum to afford PVP complex of C_{60} (**C_{60}/PVP**) and **P1–3**.

Detection of ROS generation by ESR with spin-trapping method. ESR spectra were recorded on a Bruker EMX, Continuous Wave X-Band EPR spectrometer (Bruker BioSpin GmbH, Rheinstetten, Germany). Each sample was taken into 50 μL Blaubrand® intraMark capillaries (Brand GMBH, Wertheim, Germany) and placed inside the Suprasil® ESR tube with a diameter of 4 mm, length of 250 mm, and a wall thickness of 0.8 mm (SP Wilmad-Lab Glass, New Jersey, US) for measurement. 4-Oxo-TEMP was purchased from ABCR (Karlsruhe, Germany) and purified by sublimation prior to use. DEPMPO was purchased from Enzo Life Sciences AG (Farmingdale, NY, USA) and used as it is. L-Histidine, DETAPAC, DMSO, and NADH were purchased from Sigma-Aldrich (St. Louis, Missouri, USA). Light irradiation was performed by green LED light (Lumitronix, PowerBar V3, true green, 528 nm, 93 lm W^{-1}) with a diameter of 8.5 cm. ESR measurement conditions: microwave frequency 9.78 GHz, microwave power 10 mW, receiver gain 5.02 × 10^4, modulation amplitude 1.00 G, modulation frequency 100 kHz, 10 scan average, sweep time 83.89 s. All measurements were repeated 3 times.

For $^1O_2$ measurement, a mixture (50 μL) containing PVP complex of **1–3** (**P1–3**) or C_{60} (40 μM) and 4-oxo-TEMP (80 mM) in phosphate buffer (60 mM, pH 7.0) was prepared and O_2 was bubbled for 30 s right before placing into the capillary. Each sample solution was then irradiated and the X-band ESR spectrum was recorded immediately.

For $O_2^{\bullet-}$ measurement, a mixture (50 μL) containing PVP complex **P1–3** or **C_{60}/PVP** (40 μM), DETAPAC (1 mM), NADH (10 mM), L-histidine (10 mM), and DEPMPO (113 mM) in phosphate buffer (60 mM, pH 7.0) containing 20% (v/v) DMSO was prepared and O_2 was bubbled for 30 s right before placing into the capillary. Each sample solution was then irradiated and the X-band ESR spectrum was recorded immediately.

DNA cleavage assay. Supercoiled plasmid pBR322 DNA (New England Biolabs) was used as a DNA substrate. A mixture (20 μL solution) of pBR322 (25 μg mL^{-1}), PVP complex of **1–3** (**P1–3**) or C_{60} (0.125 mM), and NADH (10 mM) was prepared in Tris–HCl buffer (10 mM, pH 8.0) containing 1 mM EDTA. Each solution was taken into round bottom 96-well microliter plate and irradiated green LED light (with 527 nm max) for 15 min by Lumidox® II 96-well LED Array (Analytical Sales and Services, Inc., New Jersey, USA). Subsequently, 4 μL of Gel Loading Dye, Purple (6×) (New England Biolabs) was added to each solution before loading to an agarose gel. Gel electrophoreses were performed in 0.5× TBE buffer at 100 V for 80 min. The gels were stained with GelRed® (Millipore) and visualized by gel imaging system (ChemiDoc, BioRad). The analysis of the images was performed using ImageJ for quantification.

Computational details

Geometry optimizations was performed employing the range-separated functional from Handy and coworkers' CAM-B3LYP[50] and Ahlrichs' Def2-SVP basis set.[51,52] The empirical dispersion D3 correction with Becke–Johnson damping was employed.[53–55] Vertical excitation energies were calculated with the same functional and basis set using Tamm–Dancoff approximation (TDA) formalism.[56] This method was proven to give accurate results for charge transfer process involving fullerenes.[57] Solvent effects were estimated using COSMO-like polarizable continuum model[58,59] in monopole approximation considering water as solvent. The chosen model demonstrated excellent performance towards the solvation energy prediction for both, neutral and charged fullerene-based systems.[60–62] Calculations were performed with the Gaussian 16 (rev. C01)[63] and Orca 5.0.3 programs.[64] Full computational details including how **P1–3** and NADH were modelled can be found in the ESI.†

Data availability

The data supporting this article have been included as part of the ESI.†

Author contributions

The manuscript was written through contributions of all authors. All authors have given approval to the final version of the manuscript.

Conflicts of interest

There are no conflicts to declare.

Acknowledgements

We are grateful for financial support from the Spanish Ministerio de Ciencia, Innovación y Universidades (MCIN/AEI/10.13039/50110001103) (Projects PID2023-147424NB-I00, PID2023-146849NB-I00, RED2022-134939-T, and FPI predoctoral grant to CC) and the Generalitat de Catalunya (Project 2021-SGR-623 and ICREA Academia 2024 prize to MS). AJS is grateful to Poland's high-performance computing infrastructure PLGrid (HPC Centers: ACK Cyfronet AGH) for providing computer facilities and support within computational grant no. PLG/2023/016841. YY is grateful to the Swiss National Science Foundation (projects 173018 and 183660).

Notes and references

1 M. Overchuk, R. A. Weersink, B. C. Wilson and G. Zheng, Photodynamic and Photothermal Therapies: Synergy Opportunities for Nanomedicine, *ACS Nano*, 2023, **17**, 7979–8003.
2 J. Rani and S. Roy, Recent Development of Copper(II) Complexes of Polypyridyl Ligands in Chemotherapy and Photodynamic Therapy, *ChemMedChem*, 2023, **18**, e202200652.
3 M. Piksa, C. Lian, I. C. Samuel, K. J. Pawlik, I. D. W. Samuel and K. Matczyszyn, The role of the light source in antimicrobial photodynamic therapy, *Chem. Soc. Rev.*, 2023, **52**, 1697–1722.
4 R. V. Huis In 't Veld, J. Heuts, S. Ma, L. J. Cruz, F. A. Ossendorp and M. J. Jager, Current Challenges and Opportunities of Photodynamic Therapy against Cancer, *Pharmaceutics*, 2023, **15**, 330.
5 M. Kolarikova, B. Hosikova, H. Dilenko, K. Barton-Tomankova, L. Valkova, R. Bajgar, L. Malina and H. Kolarova, Photodynamic therapy: Innovative approaches for antibacterial and anticancer treatments, *Med. Res. Rev.*, 2023, **43**, 717–774.
6 W. Jiang, M. Liang, Q. Lei, G. Li and S. Wu, The Current Status of Photodynamic Therapy in Cancer Treatment, *Cancers*, 2023, **15**, 585.
7 H. Abrahamse and M. R. Hamblin, New photosensitizers for photodynamic therapy, *Biochem. J.*, 2016, **473**, 347–364.
8 R. R. Allison, G. H. Downie, R. Cuenca, X.-H. Hu, C. J. H. Childs and C. H. Sibata, Photosensitizers in clinical PDT, *Photodiagn. Photodyn. Ther.*, 2004, **1**, 27–42.
9 J. W. Arbogast, A. P. Darmanyan, C. S. Foote, F. N. Diederich, R. L. Whetten, Y. Rubin, M. M. Alvarez and S. J. Anz, Photophysical properties of sixty atom carbon molecule (C_{60}), *J. Phys. Chem.*, 1991, **95**, 11–12.
10 J. W. Arbogast, C. S. Foote and M. Kao, Electron transfer to triplet fullerene C_{60}, *J. Am. Chem. Soc.*, 1992, **114**, 2277–2279.
11 T. Nagano, K. Arakane, A. Ryu, T. Masunaga, K. Shinmoto, S. Mashiko and M. Hirobe, Comparison of Singlet Oxygen Production Efficiency of C_{60} with Other Photosensitizers, Based on 1268 nm Emission, *Chem. Pharm. Bull.*, 1994, **42**, 2291–2294.
12 E. Nakamura and H. Isobe, Functionalized Fullerenes in Water. The First 10 Years of Their Chemistry, Biology, and Nanoscience, *Acc. Chem. Res.*, 2003, **36**, 807–815.
13 J. Zhu, Z. Ji, J. Wang, R. Sun, X. Zhang, Y. Gao, H. Sun, Y. Liu, Z. Wang, A. Li, J. Ma, T. Wang, G. Jia and Y. Gu, Tumor-Inhibitory Effect and Immunomodulatory Activity of Fullerol C_{60}(OH), *Small*, 2008, **4**, 1168–1175.

14 P. Chaudhuri, A. Paraskar, S. Soni, R. A. Mashelkar and S. Sengupta, Fullerenol–Cytotoxic Conjugates for Cancer Chemotherapy, *ACS Nano*, 2009, **3**, 2505–2514.

15 C. Bingel, Cyclopropanierung von Fullerenen, *Chem. Ber.*, 1993, **126**, 1957–1959.

16 I. Lamparth and A. Hirsch, Water-soluble malonic acid derivatives of C_{60} with a defined three-dimensional structure, *J. Chem. Soc., Chem. Commun.*, 1994, 1727–1728.

17 M. Maggini, G. Scorrano and M. Prato, Addition of azomethine ylides to C_{60}: synthesis, characterization, and functionalization of fullerene pyrrolidines, *J. Am. Chem. Soc.*, 1993, **115**, 9798–9799.

18 X. Camps and A. Hirsch, Efficient cyclopropanation of C_{60} starting from malonates, *J. Chem. Soc., Perkin Trans. 1*, 1997, 1595–1596.

19 M. Brettreich, S. Burghardt, C. Böttcher, T. Bayerl, S. Bayerl and A. Hirsch, Globular Amphiphiles: Membrane-Forming Hexaadducts of C_{60}, *Angew. Chem., Int. Ed.*, 2000, **39**, 1845–1848.

20 S. Bosi, T. Da Ros, G. Spalluto, J. Balzarini and M. Prato, Synthesis and Anti-HIV properties of new water-soluble bis-functionalized[60]fullerene derivatives, *Bioorg. Med. Chem. Lett.*, 2003, **13**, 4437–4440.

21 A. M. Cassell, C. L. Asplund and J. M. Tour, Self-Assembling Supramolecular Nanostructures from a C_{60} Derivative: Nanorods and Vesicles, *Angew. Chem., Int. Ed.*, 1999, **38**, 2403–2405.

22 T. Komatsu, A. Nakagawa and X. Qu, Structural and Mutagenic Approach to Create Human Serum Albumin-Based Oxygen Carrier and Photosensitizer, *Drug Metab. Pharmacokinet.*, 2009, **24**, 287–299.

23 M. Serda, G. Szewczyk, O. Krzysztyńska-Kuleta, J. Korzuch, M. Dulski, R. Musioł and T. Sarna, Developing [60] Fullerene Nanomaterials for Better Photodynamic Treatment of Non-Melanoma Skin Cancers, *ACS Biomater. Sci. Eng.*, 2020, **6**, 5930–5940.

24 O. B. Danilov, I. M. Belousova, A. A. Mak, V. P. Belousov, A. S. Grenishin, V. M. Kiselev, A. V. Kris'ko, A. N. Ponomarev and E. N. Sosnov, Generation of singlet oxygen with the use of optically excited fullerenes and fullerene-like nanoparticles, *Opt. Spectrosc.*, 2003, **95**, 833–842.

25 G. P. Tegos, T. N. Demidova, D. Arcila-Lopez, H. Lee, T. Wharton, H. Gali and M. R. Hamblin, Cationic fullerenes are effective and selective antimicrobial photosensitizers, *Chem. Biol.*, 2005, **12**, 1127–1135.

26 L. Huang, M. Terakawa, T. Zhiyentayev, Y.-Y. Huang, Y. Sawayama, A. Jahnke, G. P. Tegos, T. Wharton and M. R. Hamblin, Innovative cationic fullerenes as broad-spectrum light-activated antimicrobials, *Nanomed. Nanotechnol. Biol. Med.*, 2010, **6**, 442–452.

27 M. B. Spesia, M. E. Milanesio and E. N. Durantini, Synthesis, properties and photodynamic inactivation of *Escherichia coli* by novel cationic fullerene C_{60} derivatives, *Eur. J. Med. Chem.*, 2008, **43**, 853–861.

28 Y. Ma, L. Persi and Y. Yamakoshi, Synthesis and characterization of water-soluble C_{60}–peptide conjugates, *Beilstein J. Org. Chem.*, 2024, **20**, 777–786.

29 S. Aroua, E. G. V. Tiu, M. Ayer, T. Ishikawa and Y. Yamakoshi, RAFT synthesis of poly(vinylpyrrolidone) amine and preparation of a water-soluble C_{60}-PVP conjugate, *Polym. Chem.*, 2015, **6**, 2616–2619.

30 K. Liosi, A. J. Stasyuk, F. Masero, A. A. Voityuk, T. Nauser, V. Mougel, M. Solà and Y. Yamakoshi, Unexpected Disparity in Photoinduced Reactions of C_{60} and C_{70} in Water with the Generation of $O_2^{\bullet-}$ or $^1O_2$, *JACS Au*, 2021, **1**, 1601–1611.

31 D. Wang, J. Zhao, R. J. Mulder, J. Ratcliffe, C. Wang, B. Wu, J. Wang and X. Hao, Highly aqueously stable C_{60}-polymer nanoparticles with excellent photodynamic property for potential cancer treatment, *Smart Med.*, 2023, **2**, e20230033.

32 S.-B. Kim, C.-H. Kim, S.-Y. Lee and S.-J. Park, Carbon materials and their metal composites for biomedical applications: A short review, *Nanoscale*, 2024, **16**, 16313–16328.

33 P. J. Krusic, E. Wasserman, B. A. Parkinson, B. Malone, E. R. Holler Jr, P. N. Keizer, J. R. Morton and K. F. Preston, Electron spin resonance study of the radical reactivity of C_{60}, *J. Am. Chem. Soc.*, 1991, **113**, 6274–6275.

34 J. W. Arbogast and C. S. Foote, Photophysical properties of C_{70}, *J. Am. Chem. Soc.*, 1991, **113**, 8886–8889.

35 R. A. Marcus, Electron transfer reactions in chemistry. Theory and experiment, *Rev. Mod. Phys.*, 1993, **65**, 599–610.

36 R. A. Marcus, Free Energy of Nonequilibrium Polarization Systems. 4. A Formalism Based on the Nonequilibrium Dielectric Displacement, *J. Phys. Chem.*, 1994, **98**, 7170–7174.

37 Y. Yamakoshi, S. Sueyoshi, K. Fukuhara, N. Miyata, T. Masumizu and M. Kohno, $^{\bullet}OH$ and $O_2^{\bullet-}$ Generation in Aqueous C_{60} and C_{70} Solutions by Photoirradiation: An EPR Study, *J. Am. Chem. Soc.*, 1998, **120**, 12363–12364.

38 Y. Yamakoshi, N. Umezawa, A. Ryu, K. Arakane, N. Miyata, Y. Goda, T. Masumizu and T. Nagano, Active Oxygen Species Generated from Photoexcited Fullerene (C_{60}) as Potential Medicines: $O_2^{-\bullet}$ versus $^1O_2$, *J. Am. Chem. Soc.*, 2003, **125**, 12803–12809.

39 K. Liosi, A. Romero-Rivera, O. Semivrazhskaya, C. D. Caniglia, M. Garcia-Borràs, N. Trapp, S. Osuna and Y. Yamakoshi, Site-Selectivity of Prato Additions to C_{70}: Experimental and Theoretical Studies of a New Thermodynamic Product at the dd-[5,6]-Junction, *Org. Lett.*, 2019, **21**, 5162–5166.

40 S. Aroua, E. G. V. Tiu, T. Ishikawa and Y. Yamakoshi, Well-Defined Amphiphilic C_{60}-PEG Conjugates: Water-Soluble and Thermoresponsive Materials, *Helv. Chim. Acta*, 2016, **99**, 805–813.

41 M. Murata, Y. Murata and K. Komatsu, Surgery of fullerenes, *Chem. Commun.*, 2008, 6083–6094.

42 E. Castro, A. Artigas, A. Pla-Quintana, A. Roglans, F. Liu, F. Perez, A. Lledó, X.-Y. Zhu and L. Echegoyen, Enhanced Open-Circuit Voltage in Perovskite Solar Cells with Open-Cage [60]Fullerene Derivatives as Electron-Transporting Materials, *Materials*, 2019, **12**, 1314.

43 A. Artigas, A. Lledó, A. Pla-Quintana, A. Roglans and M. Solà, A Computational Study of the Intermolecular [2+2+2] Cycloaddition of Acetylene and C_{60} Catalyzed by Wilkinson's Catalyst, *Chem.–Eur. J.*, 2017, **23**, 15067–15072.

44 A. Artigas, A. Pla-Quintana, A. Lledó, A. Roglans and M. Solà, Expeditious Preparation of Open-Cage Fullerenes by Rhodium(I)-Catalyzed [2+2+2] Cycloaddition of Diynes and C_{60}: An Experimental and Theoretical Study, *Chem.–Eur. J.*, 2018, **24**, 10653–10661.

45 C. Castanyer, A. Pla-Quintana, A. Roglans, A. Artigas and M. Solà, Unveiling the regioselectivity of rhodium(I)-catalyzed [2+2+2] cycloaddition reactions for open-cage C_{70} production, *Beilstein J. Org. Chem.*, 2024, **20**, 272–279.

46 S. Aroua, W. B. Schweizer and Y. Yamakoshi, C_{60} Pyrrolidine Bis-carboxylic Acid Derivative as a Versatile Precursor for Biocompatible Fullerenes, *Org. Lett.*, 2014, **16**, 1688–1691.

47 Y. N. Yamakoshi, T. Yagami, K. Fukuhara, S. Sueyoshi and N. Miyata, Solubilization of fullerenes into water with polyvinylpyrrolidone applicable to biological tests, *J. Chem. Soc., Chem. Commun.*, 1994, 517–518.

48 R. A. Marcus and N. Sutin, Electron Transfers in Chemistry and Biology, *Biochim. Biophys. Acta*, 1985, **811**, 265–322.

49 C. Schweitzer and R. Schmidt, Physical Mechanisms of Generation and Deactivation of Singlet Oxygen, *Chem. Rev.*, 2003, **103**, 1685–1758.

50 T. Yanai, D. P. Tew and N. C. Handy, A new hybrid exchange–correlation functional using the Coulomb-attenuating method (CAM-B3LYP), *Chem. Phys. Lett.*, 2004, **393**, 51–57.

51 F. Weigend and R. Ahlrichs, Balanced basis sets of split valence, triple zeta valence and quadruple zeta valence quality for H to Rn: Design and assessment of accuracy, *Phys. Chem. Chem. Phys.*, 2005, **7**, 3297–3305.

52 F. Weigend, Accurate Coulomb-fitting basis sets for H to Rn, *Phys. Chem. Chem. Phys.*, 2006, **8**, 1057–1065.

53 S. Grimme, J. Antony, S. Ehrlich and H. Krieg, A consistent and accurate ab initio parametrization of density functional dispersion correction (DFT-D) for the 94 elements H-Pu, *J. Chem. Phys.*, 2010, **132**, 154104.

54 S. Grimme, S. Ehrlich and L. Goerigk, Effect of the damping function in dispersion corrected density functional theory, *J. Comput. Chem.*, 2011, **32**, 1456–1465.

55 S. Osuna, M. Swart and M. Solà, Dispersion Corrections Essential for the Study of Chemical Reactivity in Fullerenes, *J. Phys. Chem. A*, 2011, **115**, 3491–3496.

56 S. Hirata and M. Head-Gordon, Time-dependent density functional theory within the Tamm–Dancoff approximation, *Chem. Phys. Lett.*, 1999, **314**, 291–299.

57 P. Besalú-Sala, A. A. Voityuk, J. M. Luis and M. Solà, Evaluation of charge-transfer rates in fullerene-based donor–acceptor dyads with different density functional approximations, *Phys. Chem. Chem. Phys.*, 2021, **23**, 5376–5384.

58 A. A. Voityuk and S. F. Vyboishchikov, A simple COSMO-based method for calculation of hydration energies of neutral molecules, *Phys. Chem. Chem. Phys.*, 2019, **21**, 18706–18713.

59 A. A. Voityuk and S. F. Vyboishchikov, Fast and accurate calculation of hydration energies of molecules and ions, *Phys. Chem. Chem. Phys.*, 2020, **22**, 14591–14598.

60 A. J. Stasyuk, O. A. Stasyuk, M. Solà and A. A. Voityuk, Hypsochromic solvent shift of the charge separation band in ionic donor–acceptor $Li^+@C_{60}\subset$[10]CPP, *Chem. Commun.*, 2019, **55**, 11195–11198.

61 A. J. Stasyuk, O. A. Stasyuk, M. Solà and A. A. Voityuk, Electron Transfer in a Li^+-Doped Zn-Porphyrin-[10]CPP⊃Fullerene Junction and Charge-Separated Bands with Opposite Response to Polar Environments, *J. Phys. Chem. B*, 2020, **124**, 9095–9102.

62 O. A. Stasyuk, A. J. Stasyuk, M. Solà and A. A. Voityuk, [10]CPP-Based Inclusion Complexes of Charged Fulleropyrrolidines. Effect of the Charge Location on the Photoinduced Electron Transfer, *Chem.–Eur. J.*, 2021, **27**, 8737–8744.

63 M. J. Frisch, G. W. Trucks, H. B. Schlegel, G. E. Scuseria, M. A. Robb, J. R. Cheeseman, G. Scalmani, V. Barone, G. A. Petersson, H. Nakatsuji, X. Li, M. Caricato, A. V. Marenich, J. Bloino, B. G. Janesko, R. Gomperts, B. Mennucci, H. P. Hratchian, J. V. Ortiz, A. F. Izmaylov, J. L. Sonnenberg, D. Williams-Young, F. Ding, F. Lipparini, F. Egidi, J. Goings, B. Peng, A. Petrone, T. Henderson, D. Ranasinghe, V. G. Zakrzewski, J. Gao, N. Rega, G. Zheng, W. Liang, M. Hada, M. Ehara, K. Toyota, R. Fukuda, J. Hasegawa, M. Ishida, T. Nakajima, Y. Honda, O. Kitao, H. Nakai, T. Vreven, K. Throssell, J. A. Montgomery Jr, J. E. Peralta, F. Ogliaro, M. J. Bearpark, J. J. Heyd, E. N. Brothers, K. N. Kudin, V. N. Staroverov, T. A. Keith, R. Kobayashi, J. Normand, K. Raghavachari, A. P. Rendell, J. C. Burant, S. S. Iyengar, J. Tomasi, M. Cossi, J. M. Millam, M. Klene, C. Adamo, R. Cammi, J. W. Ochterski, R. L. Martin, K. Morokuma, O. Farkas, J. B. Foresman and D. J. Fox, *Gaussian 16 Rev. C.01*, Wallingford, CT, 2016.

64 F. Neese, Software update: The ORCA program system—Version 5.0, *Wiley Interdiscip. Rev. Comput. Mol. Sci.*, 2022, **12**, e1606.